
## SWIFT-XRT-CALDB-10

Release Date: 2021-Sep-23
Prepared by: Phil Evans[1], Andrew Beardmore[1]
Document revision date: 2022-Feb-08
Affiliation: [1] University of Leicester

# SWIFT XRT CALDB RELEASE NOTE

# SWIFT-XRT-CALDB-10:

# Point Spread Function

Table P1: Files to be released:

| Filename | Mode | Grade | Release Date |
|---|---|---|---|
| swxpsf20010101v006.fits | WT & PC | All | 2021-Sep-23 |

# Scope of Document

This document describes the release of an updated *Swift*-XRT point spread function (PSF) calibration file, which is effective for the entire lifetime of *Swift*.

# Introduction

The point spread function (PSF) of the XRT was measured before launch at the Panter test facility, using image-mode data[1]. It was characterised as a Gaussian + King model, thus[2]:

$$\mathrm{PSF}(r) = W \exp(-\frac{r^2}{2\sigma^2}) + (1-W)\left[1+\left(\frac{r}{r_c}\right)^2\right]^{-\beta} \quad (1)$$

where $\sigma$ is the Gaussian width (i.e. standard deviation), $r_c$ the King function core width, $\beta$ governs the shape of the King profile wings, and $W$ is the fractional Gaussian normalisation relative to that of the King component.

After launch, the PSF was redetermined in flight using Photon Counting mode data taken from two sources (Mkn 876 and RX J0720.4-312) and the Gaussian component was deemed unnecessary[3], i.e. $W = 0$; the calibration file was updated accordingly.

This model serves as an adequate description in ordinary circumstances, but for very bright sources it appears to underpredict the flux at radii beyond $\sim$ 20–30 pixels ($\sim$45–70″). Additionally, the energy and off-axis dependence of the PSF were only poorly constrained and for the combination of high energies ($>\sim$4 keV) and large off-axis angles ($>\sim 6'$) the extrapolation of the PSF coefficients tend towards physically unlikely values.

A reevaluation of the PC mode PSF was carried out for the 2SXPS catalogue[4]. This found that reinstating the Gaussian component improved the fit, and enabled the King component to better model the extended PSF wings. The PSF thus produced dramatically reduced the number of spurious sources which the SXPS source detection algorithm identified in the wings of bright sources. The PSF produced for 2SXPS was not released as a calibration file, due to the need to carry out more rigorous analysis of the effects of this new model beyond that on the source detection system employed for the catalogue. That subsequent analysis has led to this new CALDB release.

## Mode-dependent PSF models

In all previous releases, the PSF model was assumed to be identical for the two primary XRT operating modes: Photon Counting (PC) and Windowed Timing (WT), since the origin of the function is the mirrors, not the CCD read-out method. For this new analysis, we have not assumed this and have instead analysed the PSF independently in the two modes. This yielded different best-fitting models in the two modes. This is discussed further in the 'WT Mode' section, below.

## Energy and off-axis angle dependence

The ground calibration revealed only modest evidence for evolution of the PSF with photon angle or distance from the optical axis of the telescope[2], whereas the (lower signal-to-noise) in-flight calibration revealed a rather stronger dependence[3] which was encapsulated within the calibration file which has been used since early 2005. Due to the formulation of the coefficients in the calibration file, this dependence is exaggerated for the combination of higher energy and larger off-axis angles, as shown in Fig. 1.

[1] This mode is not used in routine science operations, having no timing or spectral information.
[2] Moretti, A. et al., 2004, SPIE, 5165, 232.
[3] Moretti, A. et al., 2005, SPIE, 5898, 348.
[4] Evans, P.A., et al., 2020, ApJS, 247, 54.

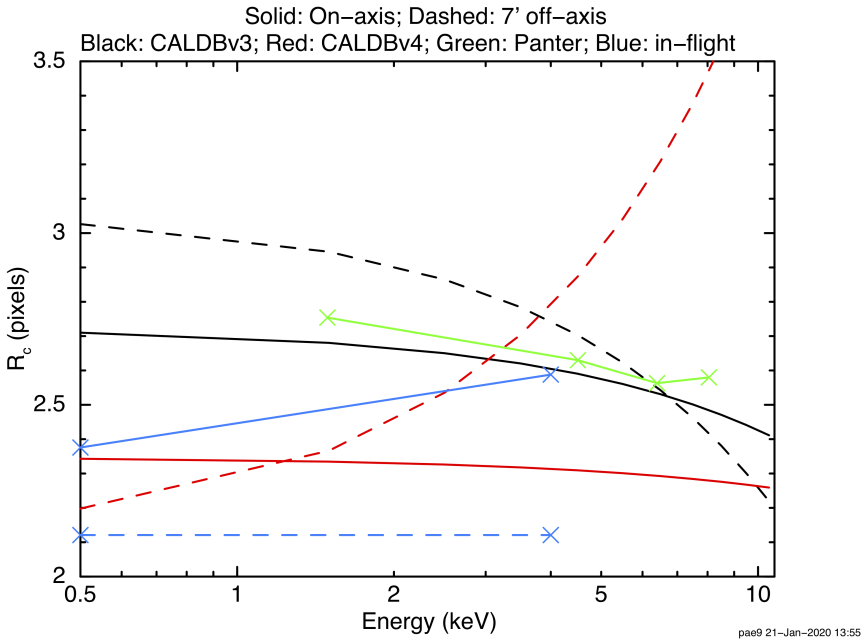


Figure 1: Energy dependence of the $R_c$ parameter in the PSF, from the previous measurements[2,3] and the previous calibration files (NB, CALDBv4 and v5 are identical in content, the v4–5 change was in internal structure).

In the revised calibration described below, we initially derived the PSF parameters without any subdivision of the data by energy or off-axis angle, in order to maximise the signal-to-noise. As a second step, we investigated whether the best-fitting parameters varied with angle or energy. No clear evidence for such dependencies were found[5]; however, the low data quality which results from subdividing the datasets prevents us from ruling out such dependence. In this new calibration file we have opted to remove all energy and off-axis angle dependence, for the following reasons:

- There is minimal evidence for such dependence in both this new calibration, and the ground calibration.
- Most sources bright enough to model well are targeted sources and so on-axis, giving limited off-axis data.
- The XRT effective area drops off steeply above 2 keV, so only a single PSF measurement can be obtained in the 2–10 keV interval.
- This combination of few measurements and the form of the dependence tends to exaggerate the variation in PSF parameters at high energy or large off-axis angles (as can be seen in Fig. 1).

As will be discussed below ('Evaluation of the new PSF'), we investigated the impact of this change by fitting a range of datasets with these new PSF profiles and the previous versions and comparing these results with those obtained by other X-ray facilities. We find no causes for concern related to the removal of these dependencies.

## PSF analysis

In order to model the PSF as accurately as possible, account must be taken for the way in which X-ray events detected by the XRT are assigned coordinates. When an event is identified, the physical CCD pixel in which that event was centred is determined. To avoid artifacts caused by pixel quantisation, the event's position is then randomised within the pixel, with a random offset uniformly distributed in the range $(-0.5, 0.5]$ determined independently for each CCD axis. This randomly-adjusted position is then converted into (RA, Dec) using the time-dependent spacecraft attitude information. It should be noted that this randomisation will result in a slight

[5]WT data are always obtained for on-axis sources, thus the off-axis angle dependence can only be studied for PC mode.

broadening of the PSF when considered in (RA, Dec) compared to that in detector coordinates, because *for photons from the source of interest* the distribution of arrival locations within a pixel is not uniform, but follows the PSF shape. That is, photons from the source are more likely to strike the side of the pixel nearest to the source, whereas the randomisation assumes that all points in the pixel are equally likely (for background photons this uniform randomisation is correct). Since data are always analysed in (RA, Dec), not detector coordinates, it is this slightly broadened PSF that we need to calibrate.

An additional complication arises in the astrometric accuracy of the *Swift* attitude information. While the changes in attitude during a continuous pointing ('snapshot') are well-tracked, the absolute attitude information has a 90% confidence uncertainty of $3.5''$[6], which is significantly larger than the XRT pixels ($2.357''$ to a side). Thus, when measuring the PSF we have to determine the source position in the XRT coordinate frame for each snapshot independently and correct for any changes, to prevent artificial broadening of the PSF (restricting ourselves to data from single snapshots would yield insufficient photons for adequate PSF measurement, certainly in PC mode). As discussed in the following sections, for PC mode this was accomplished by creating a series of sky-coordinate images, one per snapshot, and fitting the PSF model to these simultaneously. For WT mode, the different snapshots were combined into a single image using a shift-and-add technique. This latter approach involves randomising the position of each event within the pixel in which it was detected, thus the shifting and the fitting must be carried out in detector coordinates so that the positions have been randomised once (analogous to the sky-coordinate images), otherwise the data will be have been randomised twice (once by the shift-and-add, and once in the conversion to sky coordinates), and hence broadened compared to normal science data.

## PC Mode

The method employed to measure the PC-mode PSF parameters was detailed in Appendix B of the 2SXPS catalogue paper[4], and will only be summarised briefly here. Note that for 2SXPS, we used only grade 0 PC mode events (to help minimise pile up) and omitted vignetting from the exposured maps (erroneously). Given that most science analyses use grades 0-12, and that vignetting is non-zero (though very small towards the XRT boresight), for the production of this new CALDB file we redid the 2SXPS analysis using grades 0-12 and including vignetting.

We selected a set of sources in the 1SXPS catalogue with total-band count rates in the range 0.3–0.6 ct $s^{-1}$, a minimum of five separate observations in the catalog, and a Galactic absorption column below $3\times10^{21}$ $cm^{-2}$. The latter criterion was to reduce the risk of high foreground dust contamination which can broaden the PSF by scattering. Fits were performed out to a radius of 100 pixels, unless there was a contaminating source nearby in which case the radius was reduced. The selected sources and fit details are listed in Table 1. For each source, we identified the observations in the 1SXPS catalogue containing the source, and split them into snapshots[7], determining for each the centroid (in the XRT coordinate frame) and rejecting any where the 1-$\sigma$ statistical error on this centroid was above 0.5 pixels. We then fitted the PSF model from equation 1, with an extra free parameter representing the background level, to all the remaining snapshots for the source simultaneously, using a simulated annealing method to alleviate problems with local minima. This yielded 22 measurements of the PSF parameters and their uncertainties (i.e. one for each source). We combined these into probability distribution functions. The central limit theorem tells us that these should be Gaussian in nature, so we modelled them as such to find the best-fitting PC mode PSF parameters, as given in Table 2.

As can be seen (and as reported for 2SXPS), we find that a Gaussian component is necessary; its inclusion improving the modelling of the PSF core, particularly at 8–15 pixels, which in turn allows the King component to broaden, better reproducing the wings (see Fig. 2). We also found that the background level from these fits was slightly lower than obtained using the King-only function – this is the expected result demonstrating that the wings of the PSF are broader than previously believed. The background levels fitted were consistent with the typical background measurements found for 1SXPS (and 2SXPS) fields.

## WT mode

One benefit of using WT mode to characterise the PSF is its faster readout time (1.78 ms) means brighter sources can be used, allowing the wings of the PSF to be probed while avoiding pile-up in the core. The faster readout time is achieved by continuously clocking 10 parallel rows at a time into the serial register, then reading the central

[6] see SWIFT-XRT-CALDB-06.

[7] A snapshot is a period of continuous observations with XRT. Snapshots are terminated either by the source being eclipsed by the Earth due to the satellite orbit, or Swift slewing to another target.

Table 1: Sources used to determine the PC-mode PSF

| Source ID | RA (J2000) | Dec (J2000) | Fit radius (pixels) |
|---|---|---|---|
| 1SXPS J164607.0+422736 | 251.5295 | +42.4602 | 70 |
| 1SXPS J035141.5-402759 | 57.9233 | -40.4666 | 100 |
| 1SXPS J142725.0+194952 | 216.8545 | +19.8312 | 55 |
| 1SXPS J012732.3+191042 | 21.8849 | +19.1786 | 100 |
| 1SXPS J012806.6-184831 | 22.0279 | -18.8088 | 45 |
| 1SXPS J031118.9-204618 | 47.8288 | -20.7719 | 70 |
| 1SXPS J112048.0-431552 | 170.2000 | -43.2647 | 100 |
| 1SXPS J134112.8-143839 | 205.3036 | -14.6444 | 100 |
| 1SXPS J213227.7+100816 | 323.1158 | +10.1380 | 80 |
| 1SXPS J091552.2+293323 | 138.9678 | +29.5566 | 100 |
| 1SXPS J141650.1-115859 | 214.2088 | -11.9831 | 100 |
| 1SXPS J185649.2-544229 | 284.2053 | -54.7081 | 90 |
| 1SXPS J012910.8-214202 | 22.2954 | -21.7006 | 100 |
| 1SXPS J044122.5-270820 | 70.3441 | -27.1389 | 80 |
| 1SXPS J220907.5-274834 | 332.2814 | -27.8096 | 70 |
| 1SXPS J003620.8+453951 | 9.0868 | +45.6644 | 75 |
| 1SXPS J184229.8-584159 | 280.6245 | -58.6998 | 100 |
| 1SXPS J003417.2-790518 | 8.5721 | -79.0883 | 50 |
| 1SXPS J073656.9+584612 | 114.2374 | +58.7700 | 90 |
| 1SXPS J040748.6-121134 | 61.9528 | -12.1929 | 100 |
| 1SXPS J021437.4-643003 | 33.6560 | -64.5010 | 100 |
| 1SXPS J013445.5-043014 | 23.6897 | -4.5040 | 85 |

Table 2: The best-fitting PSF parameters for PC mode; see equation 1 for definitions of the parameters. $r_c$ and $\sigma$ values are in XRT pixels; 1 pixel = 2.357″.

| Parameter | Value |
|---|---|
| $W$ | $0.075^{+0.034}_{-0.024}$ |
| $\sigma$ | $3.15 \pm 0.23$ |
| $r_c$ | $1.58 \pm 0.20$ |
| $\beta$ | $1.305 \pm 0.079$ |

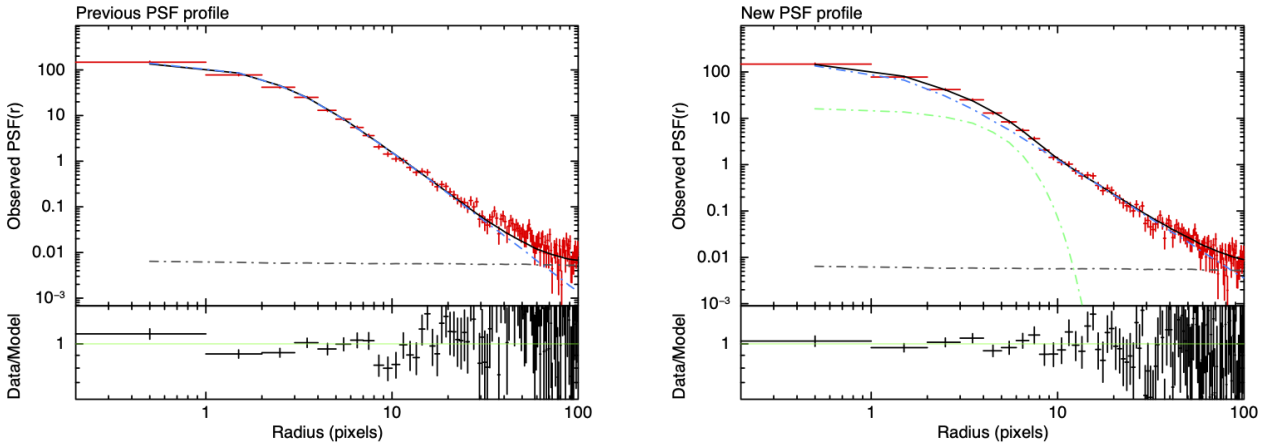


Figure 2: A comparison of the old (left) and new PSF (right) profiles in PC mode. The radial intensity profile of 1SXPS J112048.0-431552 is shown in red with the best-fitting PSF model in black. The King (blue) and Gaussian (green; new only) component are also shown individually. The improvement both in the core and wings is clearly see in the ratio plot (lower panes).

Table 3: The best-fitting PSF parameters for WT mode; see equation 1 for definitions of the parameters. $r_c$ and $\sigma$ values are in XRT pixels; 1 pixel = 2.357″.

| Source | Exposure[a] | $N_H$[b] | $r_c$ | $\beta$ |
|---|---|---|---|---|
| Mrk 421($< 2'$) | 76.0 | 2.0 | $2.021 \pm 0.003$ | $1.452 \pm 0.001$ |
| Mrk 501 | 131.9 | 1.6 | $1.933 \pm 0.008$ | $1.433 \pm 0.002$ |
| Her X-1 | 20.0 | 1.8 | $1.926 \pm 0.008$ | $1.415 \pm 0.003$ |
| MAXIJ1820 | 9.0 | 2.0 | $1.933 \pm 0.023$ | $1.385 \pm 0.006$ |
| average | | | $1.953 \pm 0.023$ | $1.421 \pm 0.014$ |

[a] Accumulated exposure time (ks); [b] Source column density ($\times 10^{20}\,\mathrm{cm}^{-2}$);

200 pixels only from the latter. This effectively produces a 1D readout 200 pixels wide in the detector X direction (DETX), as the detector Y dimension (DETY) is summed into the serial register. When modelling the 1D source profiles returned by the WT mode readout the PSF was treated appropriately, with the 2D profile summed in the DETY direction to mimick the WT readout.

Observations of a number of sources from the UKSSDC archive were chosen which had a low line-of-sight column density in order to minimise the possibility of PSF broadening from dust scattering halo effects. In particular, Mrk 421 and Her X-1 were selected, which have been used by other researchers to confirm the Chandra HRMA PSF profile (e.g. Costantini et al 2005 AA 444 187, Corrales & Paerels 2015 MNRAS 453 1121).

Given an appropriate target, the procedure used to characterise the WT PSF was as follows:

- Use XRT snapshots with grade 0 count rates $< 90$ count $\mathrm{s}^{-1}$ (to be free from pile-up) and taken within 3 arcminutes of the centre of the field-of-view (to minimise the effects of telescope vignetting variations).
- Reject the first 50 s of data from a snapshot to ignore the possible few arcsecond attitude drift sometimes seen when the spacecraft settles onto a new target.
- Extract 1D profiles in the detector X (DETX) dimension from consecutive 30 s intervals throughou the snapshot.
- Mimick the 1D WT readout by calculating the 2D PSF model then collapse it down (i.e. sum over 600 pixels) in the detector Y (DETY) direction.
- Fit for the source DETX centroid position. (Note, the source DETY position, required for the 2D model centre, is predicted from the spacecraft attitude and telescope/CCD alignment using the *pointxform* FTOOL.)
- Shift-and-stack the 30 s profiles, randomising events over the finite pixel width when doing so.
- Take the final stacked profile and simultaneously fit for the PSF model parameters and an additional background level, allowing a $\pm 1$ dex range on the latter (as the WT background has been slowly increasing with time from $\sim 0.001 - 0.01$ count/s/column).

The measured King function parameters for the individual sources and their average are shown in table 3. The results are exemplified by Fig. 3, which compares the WT profile fits obtained to the Her X-1 data for the CALDB v005 PSF model parameters (left hand panels) and the new v006 PSF parameters (right hand panels). The measured profile wings are broader than that predicted by the v005 PSF model, which causes the modelled background level to increase to compensate, resulting in 'M' shaped ratio residuals. The v006 PSF models the data better, leading to flatter residuals and a lower background level (which is more consistent with other background estimates for the epoch of WT data considered here).

We note that the WT PSF model presented here utilises the King component only as it was found to produce a flatter data/model residuals ratio out beyond 100 pixels radius overall. Although a King + Gaussian model could give a statistically better fit (due to the larger concentration of counts in the PSF core and its dominant effect on the fit statistic), the data/model ratio was then worse in the wings at larger radii ($\gtrsim 30$ pixels) compared to the King only fit, as it altered the King function $\beta$ parameter sufficiently that it no longer modelled the wings as well.

There is some evidence from WT mode that the optimal model may require an additional component (e.g. a King and *two* Gaussians); the two differing models for PC & WT thus arise because the different modes probe

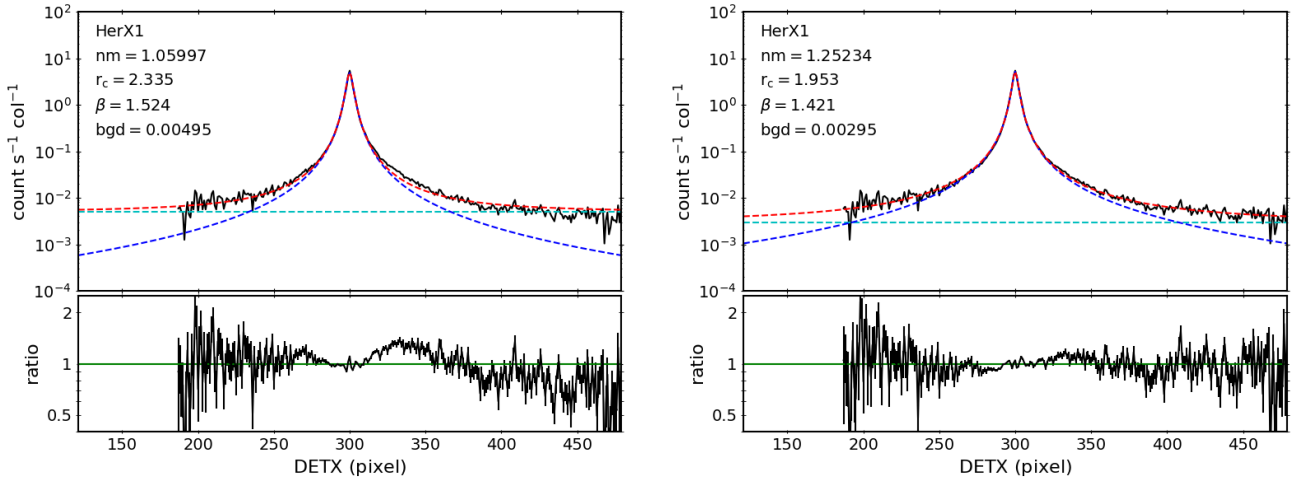


Figure 3: Observed WT 1D profile from Her X-1 observed from data taken between 2012–2017 (exposure 20ks). The observed profile is fit with the CALDB v005 PSF model on the left and the v006 WT PSF model on the right. The blue curves show the modelled PSF component, the cyan lines the fitted background level and the red the total model.

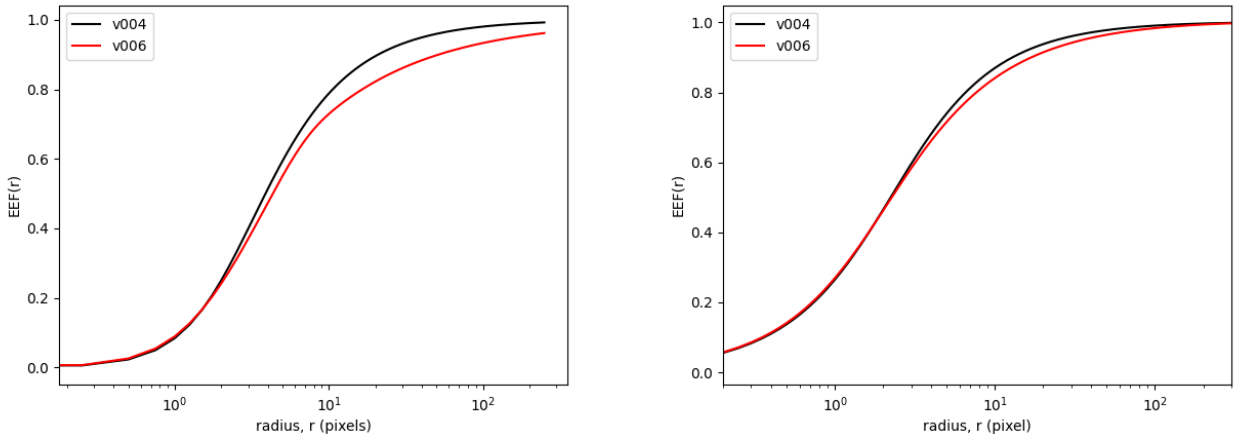


Figure 4: The EEF in the previous CALDB release (black) and this new file (red). **Left**: PC mode. **Right**: WT mode.

different count rate regimes which alters the relative effect and importance of the various components in the fitting procedure. To support the King + Gauss + Gauss model would require a significant revision of the XRT analysis software, and the parameters would be difficult to accurately constrain for PC mode (due to the faintness of the sources required to avoid pile-up); therefore we do not believe this is necessary.

## Comparison with the previous PSF

The encircled energy function (EEF) is the integral of the PSF, and shows the fraction of source energy enclosed as a function of radius. The broadening of the PSF wings in this new release naturally results in a slightly flattened EEF, as shown in Fig. 4. The impact of this obviously depends on the size and shape (e.g. circular or annular) of the region over which source counts were accumulated, but for typical sources will result in a small ($\sim 10\%$ for PC mode; $\sim 5\%$ for WT mode) increase in absolute flux.

The removal of energy dependence also has a potential impact on the results obtained using this new PSF, although again the exact nature of this will depend on the source's spectrum, off-axis angle, and the extraction region used.

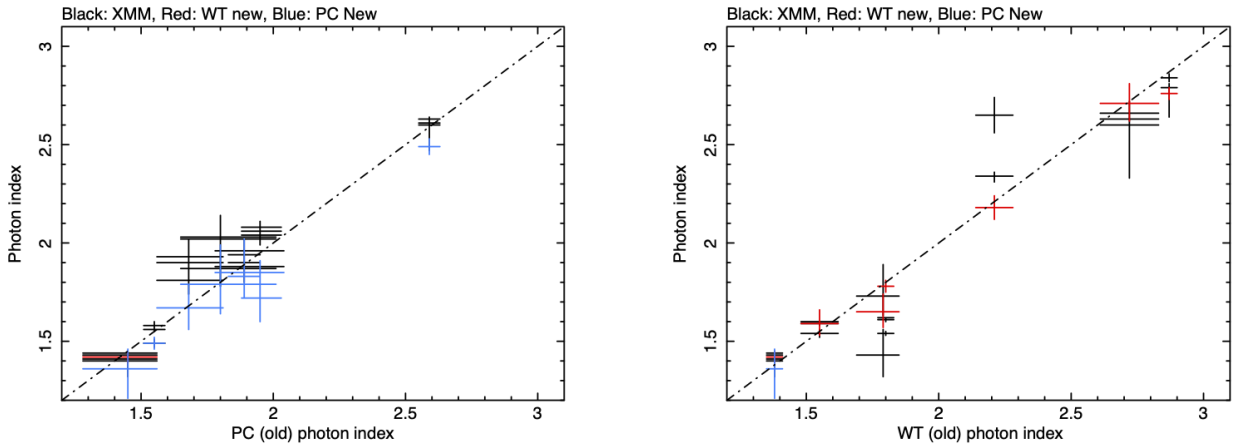


Figure 5: A comparison of the spectral results obtained using the new and old PSFs, and from *XMM-Newton* data. **Left**: PC mode. **Right**: WT mode.

To investigate in more detail, we analysed a selection of AGN and GRB which were observed simultaneously by *Swift* and *XMM-Newton*. Fig. 5 shows a comparison of the power-law spectral photon index obtained in these fits; the x-axis shows the value obtained fitting the XRT data using the previously-released CALDB. On the y-axis is shown the values from XRT using the new PSF, and also the values obtained from *XMM*. As can be seen, there is significant scatter in the results, demonstrating the cross-calibration uncertainties. In many cases, the new PSF gives better agreement with *XMM*, in some the agreement is slightly worse. Analysis of observations carried out for cross calibration with other facilities under the auspices of IACHEC showed similar results. We thus conclude that the removal of energy dependence from the PSFs eliminates the exaggerated effects seen in Fig. 1, and shows no significant change in agreement with results from *XMM*.

# Limitations

The PSF profiles derived here are appropriate for point sources and not suitable for sources (such as SNRs like the Crab) that show extensions to their surface brightness profiles, for which a dedicated analysis will be required outside XRTMKARF.

It is not uncommon for interstellar dust clouds to lie between Earth and a given target, especially when observations are performed close to the Galactic plane. X-rays not originally destined for the Earth can scatter off these clouds and back towards the Earth, and as a result the original object becomes extended and no longer point-like. In the extreme case of a bright and variable source like V404 Cygnii, the dust scattered X-rays are visible as rings surrounding the central source[8]. However, in most cases the broadening is not obvious, but nonetheless, the observed PSF is broader in the wings than expected for a genuine point source.

For this calibration, we deliberately chose objects with low Galactic column densities ($\lesssim 10^{21}\,\mathrm{cm}^{-2}$) to ensure that we were measuring the narrowest point spread function. However, when observing sources with large Galactic columns (e.g. MAXIJ1535-571), users should bear in mind that the source may be extended and, in this case, XRTMKARF provided PSF corrections can be underestimated when compared to instruments with more limited spatial resolution which gather a larger fraction of the scattered flux, requiring a constant factor significant larger than one when joint spectral fits are performed.[9].

[8]For example, Heinz et al. 2016 ApJ 825 15, Beardmore et al., 2016, MNRAS, 462, 1847
[9]See, for example, Corrales et al. 2016 MNRAS 458 1345; Jin et al. 2019 ApJ 875 157

## Useful Links

| | |
|---|---|
| XRT analysis threads at the UKSSDC, University of Leicester | http://www.swift.ac.uk/XRT.shtml |
| XRT digest pages at the UKSSDC, University of Leicester | http://www.swift.ac.uk/xrtdigest.shtml |
| XRT analysis at GSFC | http://swift.gsfc.nasa.gov/docs/swift/analysis |
| IACHEC website | http://web.mit.edu/iachec/ |